

Experimental and theoretical studies of 3-benzyloxy-2-nitropyridine

Wenting Sun, Yu Cui, Huimin Liu, Haitao Zhao*, Wenqin Zhang*

Department of Chemistry, School of Science, Tianjin University, Tianjin 300072, China

HIGHLIGHTS

- ▶ Synthesis of 3-benzyloxy-2-nitropyridine.
- ▶ The compound was characterized by IR, Raman and X-ray crystallography.
- ▶ DFT studies on the structures of the compound.
- ▶ DFT studies on the vibrational frequencies.

ARTICLE INFO

Article history:

Received 20 March 2012
Received in revised form 23 May 2012
Accepted 23 May 2012
Available online 6 June 2012

Keywords:

3-Benzyloxy-2-nitropyridine
Crystal structure
Theoretical studies
Rotational barrier
Vibrational spectra

ABSTRACT

The structure of 3-benzyloxy-2-nitropyridine has been investigated both experimentally and theoretically. The X-ray crystallography results show that the nitro group is tilted out of the pyridine ring plane by $66.4(4)^\circ$, which is mainly attributed to the electron–electron repulsions of the lone pairs in O atom of the 3-benzyloxy moiety with O atom in nitro group. An interesting centrosymmetric π -stacking molecular pair has been found in the crystalline state, which results in the approximate coplanarity of the pyridine ring with the benzene ring. The calculated results show that the dihedral angle between the nitro group and pyridine ring from the X3LYP method is much closer to the experimental data than that from the M06-2X one. The existing two conformational isomers of 3-benzyloxy-2-nitropyridine with equal energy explain well the disorder of the nitro group at room temperature. In addition, the vibrational frequencies are also calculated by the X3LYP and M06-2X methods and compared with the experimental results. The prediction from the X3LYP method coincides with the locations of the experimental frequencies well.

© 2012 Elsevier B.V. All rights reserved.

1. Introduction

In the aromatic nitro compounds without *o*-substituent group, the nitro groups are usually coplanar with the aromatic ring planes, in which the dihedral angles between the nitro groups and the aromatic ring planes are less than 5° [1–3]. In these cases, the molecules are stabilized by the *p*– π conjugation. However, the dihedral angles between the nitro group and the aromatic ring planes are varied from 10° to 70° in some *o*-substituted aromatic nitro compounds [4–6], and even to about 90° in some *o,o'*-disubstituted ones such as $84(1)^\circ$ in 1,3,5-triisopropyl-2-nitrobenzene [7]. The large dihedral angle is generally attributed to the steric effect of the *o*-substituent [8]. For example, in 2-[(4-methylphenylimino)methyl]-1-nitrobenzene, the nitro plane is tilted out of the benzene ring plane by $27.9(5)^\circ$ to minimize the steric hindrance between the ortho atoms of the nitro group and their vicinal H atoms [9].

The molecular structures of 3- and 4-nitropyridine derivatives have been extensively reported [10,11]. However, the molecular structures of 2-nitropyridine derivatives are seldom investigated. The title compound, 3-benzyloxy-2-nitropyridine (**BNP**, Scheme 1), is an important intermediate for the synthesis of asymmetric cyanine dyes for the fluorescence detection of nucleic acids [12]. In this paper, the molecular structure of **BNP** was determined by X-ray single crystallography. The nitro group is disordered, and a very large dihedral angle (66.4°) between the nitro group and the pyridine ring plane was observed. In order to explain these observations, the molecular structure and the rotational barrier of the nitro group were studied theoretically. Moreover, the vibrational spectra of **BNP** were calculated by the X3LYP [13,14] and M06-2X [15] methods.

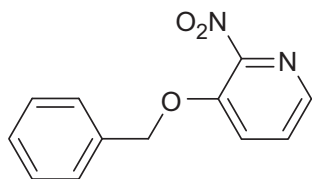
2. Experimental and theoretical methods

2.1. Materials and general methods

All reagents are commercially available and purified by standard methods prior to use. The melting points were measured on

* Corresponding authors. Tel.: +86 22 58269011; fax: +86 22 27403475.

E-mail addresses: htzhao@tju.edu.cn (H. Zhao), wqzhang@tju.edu.cn (W. Zhang).



Scheme 1.

Table 1
Crystal data and structure refinement summary for BNP.

Empirical formula	C ₁₂ H ₁₀ N ₂ O ₃
Formula weight	230.22
Crystal system	Monoclinic
Space group	P2 ₁ /n
<i>a</i> (Å)	7.112(3)
<i>b</i> (Å)	13.030(6)
<i>c</i> (Å)	12.407(5)
β (°)	92.004(7)
<i>V</i> (Å ³)	1149.0(9)
<i>D_c</i> (g/cm ³)	1.331
<i>F</i> (000)	480
<i>Z</i>	4
μ (MoK α)/mm	0.098
θ Range (°)	2.27–25.00
Range of <i>h, k, l</i>	–7/8, –15/13, –14/13
Reflections collected/unique	5774/2029
Data/restraints/parameters	2029/36/172
<i>R</i> and <i>wR</i>	0.0510 and 0.1522
Goodness-of-fit on <i>F</i> ²	1.022
Max. res. peak and hole (e Å ^{–3})	0.131 and –0.185

Table 2
Selected bond lengths (Å) and bond angles (°) for BNP from the experiment and theoretical calculations.

Parameters	M06-2X	X3LYP	Experiment
O(2)–N(2)	1.212	1.221	1.205
O(3)–N(2)	1.204	1.214	1.220
N(2)–C(12)	1.489	1.493	1.494
N(1)–C(12)	1.304	1.309	1.315
O(1)–C(8)	1.337	1.343	1.357
O(1)–C(7)	1.421	1.432	1.431
C(6)–C(7)	1.506	1.507	1.512
O(2)–N(2)–C(12)	116.5	116.5	118.2
O(3)–N(2)–C(12)	117.1	117.2	116.3
O(2)–N(2)–O(3)	126.4	126.3	125.5
C(11)–N(1)–C(12)	117.7	118.0	115.1
C(8)–O(1)–C(7)	118.7	119.4	119.5
O(1)–C(7)–C(6)	108.3	108.8	107.8
O(2)–N(2)–C(12)–N(1)	–130.1	–125.7	–114.8
O(3)–N(2)–C(12)–N(1)	48.6	53.0	66.2
O(2)–N(2)–C(12)–C(8)	49.4	54.0	65.6
O(3)–N(2)–C(12)–C(8)	–131.9	–127.4	–113.3
N(2)–C(12)–C(8)–O(1)	3.8	3.5	1.2
C(1)–C(6)–C(7)–O(1)	–25.6	–29.8	0.8

a Yanagimoto MP-500 apparatus (uncorrected). The FT-IR spectra (KBr pellets and in CCl₄ solvent) were measured on a BIO-RAD FTS 3000 infrared spectrometer in the 4000–400 cm^{–1} range with a 4 cm^{–1} resolution. The FT-Raman spectra were measured using Bruker RFS 100/S FT-Raman spectrometer with a 4 cm^{–1} resolution. The ¹H NMR spectra were recorded on a Bruker AV-400 spectrometer (400 MHz) at 298 K in CDCl₃. The MS was performed on the Thermo Finnigan Trace DSQ GC–MS spectrometer.

2.2. Preparation of BNP

2-Nitro-3-hydroxypyridine (2.80 g, 20 mmol) was added to a solution of NaOH (0.80 g, 20 mmol) in 20 ml EtOH and stirred for

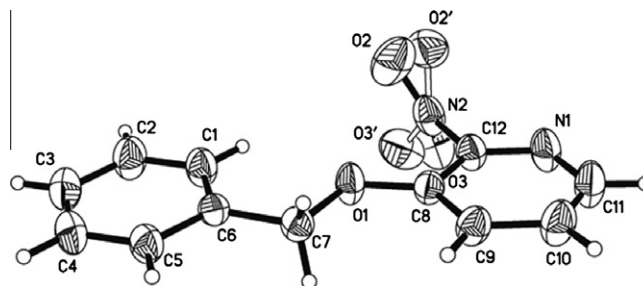


Fig. 1. The crystal structure of BNP with atom labels and 30% probability ellipsoids level.

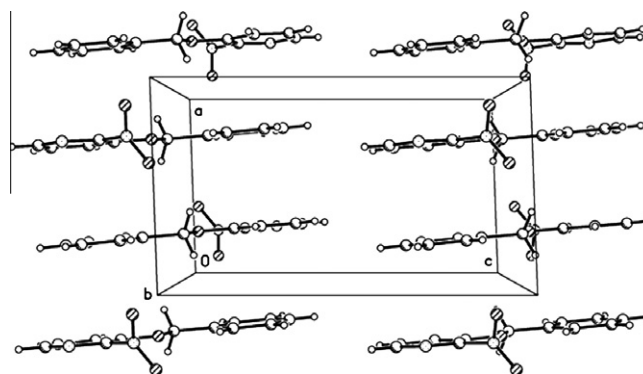


Fig. 2. The crystal packing, viewed along the *b* axis.

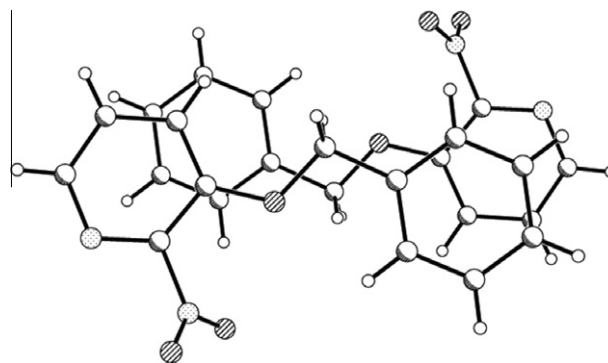


Fig. 3. The centrosymmetric π -stacking molecular pairs.

1 h at room temperature. The formed sodium salt was collected and air-dried.

A solution of benzyl bromide (2.15 ml, 18 mmol) in 18 ml DMF was added dropwise to the mixture of the above sodium salt (2.93 g, 18 mmol) in 18 ml DMF, and was stirred for 10 h at room temperature. Then the reaction mixture was added 100 ml water, extracted with ethyl ether (3 \times 100 ml). The ether phase was dried with anhydrous MgSO₄, filtrated, and concentrated to afford crude yellow liquid, which was further purified by chromatography using light petroleum/ethyl acetate (2:1) as the eluant to provide colorless needle crystals (3.03 g, 74.0%), mp. 60–62 °C. ¹H NMR (CDCl₃): δ 8.06 (d, *J* = 4.4 Hz, 1H), 7.50 (d, *J* = 8.4 Hz, 1H), 7.45 (dd, *J*₁ = 4.4 Hz, *J*₂ = 8.4 Hz, 1H), 7.41–7.31 (m, 5H). MS: *m/z* 91 (100, M⁺-NO₂PyO[–]), 124 (12.6).

2.3. X-ray crystallography

Single-crystal X-ray diffraction measurements were carried out on a Bruker Smart 1000 CCD diffractometer using graphite

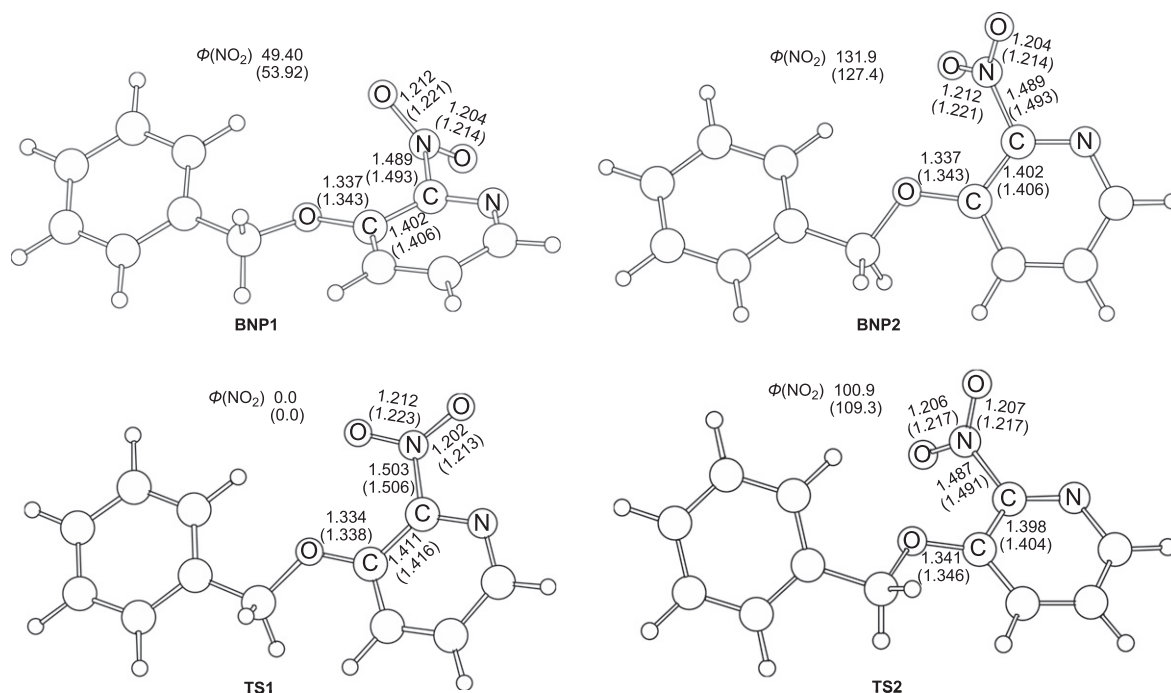


Fig. 4. The optimized structures with selected structural parameters (bond lengths in angstroms and angles in degrees) for species involved in the **BNP1** and **BNP2**. Selected calculated structural parameters for the conformers are compared with X3LYP method (in parentheses).

monochromatized MoK α radiation ($\lambda = 0.71073 \text{ \AA}$) with φ and ω scan mode at 293(2) K. Semi-empirical absorption corrections were applied using SABABS program. All structures were solved by direct method and successive difference Fourier syntheses (SHELXS-97), and refined by full-matrix least-squares procedure on F^2 with anisotropic thermal parameters for all non-hydrogen atoms (SHELXL-97) [16]. Hydrogen atoms were generated geometrically and refined with fixed thermal factors riding on the concerned atoms. The two O atoms of the nitro group are disordered over two sites. The ratio of site occupancies, from the refinement, was 0.75:0.25. Crystallographic data and experimental details for structural analyses are summarized in Table 1, and the selected bond lengths and angles are presented in Table 2.

2.4. Theoretical method

Molecular geometries of the model complexes were optimized without constraints via DFT calculations using the X3LYP and the M06-2X functionals, as implemented in the Gaussian 09 suite of programs [17]. It is known that these two functionals have good performance in the calculation of compounds having weak interactions. The 6-311G** basis set [18] was used for all atoms. Frequency calculations at the same level of theory have also been performed

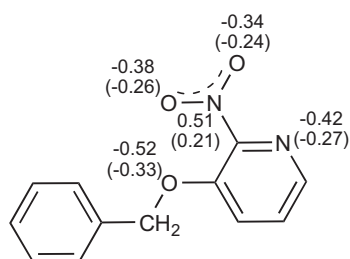


Fig. 5. The calculated NBO and Mulliken (in parentheses) charges at the X3LYP/6-311G** theoretical level.

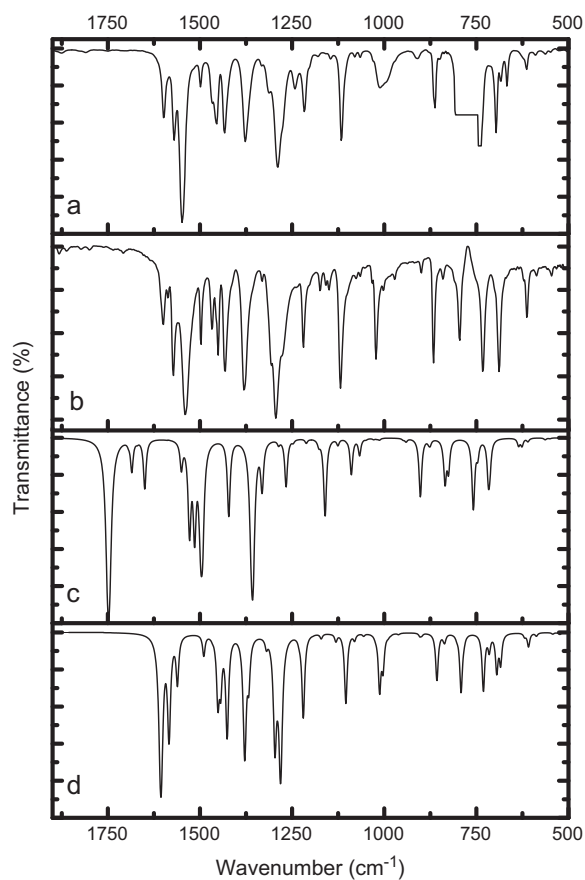


Fig. 6. The experimental IR spectra for **BNP** ($1900\text{--}500 \text{ cm}^{-1}$) in (a) CCl_4 solvent and (b) KBr pellets and compared with the computational results via the methods of (c) M06-2X and (d) X3LYP.

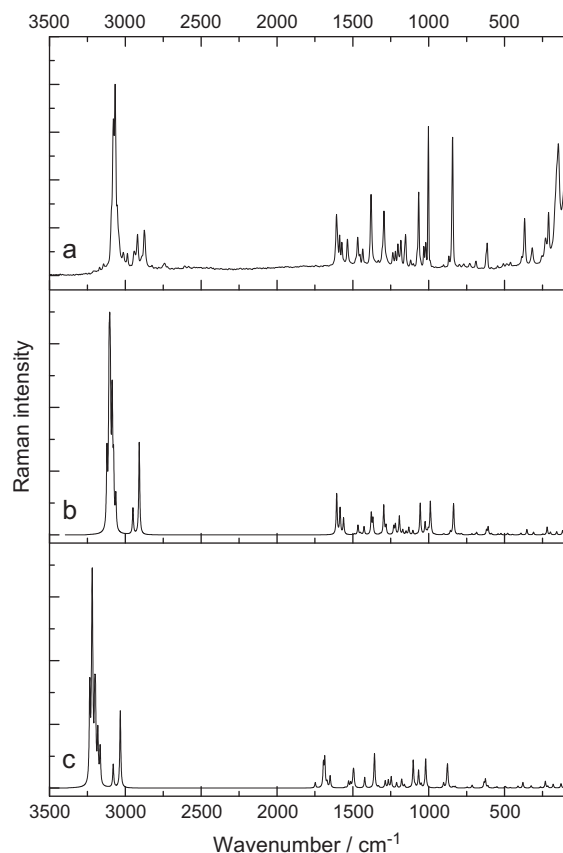


Fig. 7. The experimental Raman spectra of **BNP** and compared with the computational results via the methods of (b) X3LYP and (c) M06-2X.

to identify all of the stationary points as minima (zero imaginary frequencies) or transition states (one imaginary frequency), and to provide free energies at 298.15 K which include entropic contributions by taking into account the vibrational, rotational, and translational motions of the species under consideration. To better understand the nature of the intramolecular interaction, we performed natural bond orbital (NBO) analysis for **BNP** with the NBO 5.9 standalone package [19,20]. Furthermore, the Mulliken charge distribution was calculated via the Gaussian 09 suite of programs [17]. The vibrational frequencies were scaled by 1.0 for M06-2X/6-311G** and 0.9703 for X3LYP/6-311G** [21]. In convenience, we define the torsion angle of C8–C12–N2–O2 as $\phi(\text{NO}_2)$. It should be noted that we use gas-phase calculation to reproduce the molecular structures and vibrational frequencies of solid phase compounds.

3. Results and discussions

3.1. Crystal structure

The bond lengths and angles in **BNP** are normal (Fig. 1). Due to the p - π conjugation, the O1 atom adopts sp^2 hybridization and both of the C7 and O1 atoms are almost coplanar with the pyridine ring plane. The deviation of C7 atom from the least-squares of pyridine plane is $-0.069(5)$ Å. In addition, the torsion angle of C1–C6–C7–O1 is only $0.7(6)^\circ$. Therefore, the pyridine and the benzene rings are almost coplanar with a small dihedral angle of $-2.5(9)^\circ$. However, this quasi-planar conformation does not exist in some other benzyloxy heterocyclic compounds. For example, in 2-amino-6-benzyloxy-4-(*N*-methylamino)-5-nitrosopyrimidine [22] and 4-amino-6-benzyloxy-2-(methylsulfanyl) pyrimidine

[23], the pyrimidine ring and the benzene ring are close to perpendicular. The planar conformation of **BNP** can be explained by the π -stacking effect between the layer packing of the **BNP** molecules (Fig. 2). Such π -stacking effect between pyridine and benzene rings belongs to two **BNP** molecules prevent the rotation of benzene ring around the C6–C7 single bond. However, we found that the benzene ring is uncoplanar with the pyridine ring in the energetically favored conformation of **BNP** resulting from the theoretical calculation, in which the **BNP** molecule was considered independently. The dihedral angle of the benzene and pyridine ring planes is $-17.8(0)^\circ$ from the X3LYP method. This can further demonstrate that π -stacking effect is the main force to sustain **BNP** in a planar conformation in the crystalline state.

In the crystal structure of **BNP**, it was found that the nitro group was disordered and the site occupancy factors were refined to 0.75 (O2 or O3) and 0.25 (O2' or O3'), respectively. The nitro group is tilted out of the pyridine ring plane by a large angle of $66.4(4)^\circ$ for O2–N2–O3 and $76.4(4)^\circ$ for O2'–N2'–O3', and the two components vibrate by $37.1(4)^\circ$ from each other around the C12–N2 single bond. It seems that there exists a low rotational barrier between the two components, which is so low that the two components can vibrate from each other at room temperature. We calculated the corresponding transition states in the next section and tried to find whether the nitro group vibrates through a small barrier.

Due to the dipole–dipole interaction between the electron poor pyridine ring and electron rich benzene ring, an interesting π -stacking molecular pair of **BNP** was formed centrosymmetrically (Figs. 2 and 3) with a separation distance of $3.568(5)$ Å, which indicates the presence of C–T interactions. These centrosymmetric pairs are further assembled into layers in the overall crystal packing, as what the normal planar organic molecules show (Fig. 2).

3.2. Theoretical analysis

The observation and analysis above prompt us to calculate the rotational barriers of the nitro group, and these values may help us to explain its disorder. Through our calculation, we indeed locate two conformational isomers (**BNP1** and **BNP2**) equivalent by rotation. The $\phi(\text{NO}_2)$ for the two isomers calculated by X3LYP method is 53.9° and 127.4° , respectively. Fig. 4 shows the optimized structures with selected structural parameters for the conformational isomers **BNP1** and **BNP2**. In Table 2, the calculated structural parameters of the **BNP1** are compared with their corresponding experimental ones. The calculated geometries reproduce well the important structural parameters. For example, calculated geometric parameters for **A1** by X3LYP method, O3–N2 = 1.214 Å, N2–C12 = 1.493 Å, N1–C12 = 1.309 Å, agree well with experimentally determined values for the **BNP**, O3–N2 = 1.220 Å, N2–C12 = 1.494 Å, N1–C12 = 1.315 Å, thus confirming that the basis sets are adequate for present study. For a specific bond, we find that M06-2X calculated bond length is slightly shorter than the bond length calculated by X3LYP method. The deviation between the theoretical and experimental value of bond length is less than 0.02 Å, which suggest that the two DFT functional methods are reliable for the current study.

The current DFT calculations allow us to measure the energy barriers of conformational isomerization between isomers **BNP1** and **BNP2**. Through nitro group rotating around the C12–N2 single bond, we locate two transition states with very small barriers of 2.5 and 1.6 kcal mol $^{-1}$ from the X3LYP method, respectively. The barriers are even smaller than the C–H bond rotation in ethane along the C–C bond, which needs a barrier of 3 kcal mol $^{-1}$. From the very low barrier height (1.6 kcal mol $^{-1}$), we conclude that the nitro group can free rotate in the room temperature. The optimized

Table 3The theoretical (M06-2X 6-311G** and X3LYP 6-311G**) and experimental (KBr pellets and in CCl₄ solvent) frequencies (cm⁻¹) for BNP.

No.	Theoretical				Experimental		Assignments ^c
	X3LYP	I ^a	M06-2X	I ^a	CCl ₄ ^b	KBr pellets ^b	
1	3121	1	3234	0			$\nu_s(\text{Py-H})$
2	3107	3	3218	3			$\nu_s(\text{Ph-H})$
3	3103	7	3222	2	3092 vw	3092 w	$\nu_{as}(\text{Py-H})$
4	3098	6	3214	1			$\nu_{as}(\text{Ph-H})$
5	3088	8	3197	2	3069 w	3067 w	$\nu_{as}(\text{Ph-H})$
6	3085	1	3202	1			$\nu_{as}(\text{Py-H})$
7	3077	1	3181	0			$\nu_{as}(\text{Ph-H})$
8	3062	3	3166	1	3036 w	3036 w	$\nu_{as}(\text{Ph-H})$
9	2950	9	3080	4	2909 w	2918 w	$\nu_{as}(\text{CH}_2)$
10	2908	8	3033	4	2884 w	2874 w	$\nu_s(\text{CH}_2)$
11			1748	100			$\nu_{as}(\text{NO}_2)$
12	1607	2	1694	0			$\nu_{sk}(\text{Ph})$
13	1606	100			1599 m	1599 m	$\nu_{as}(\text{NO}_2), \nu_{sk}(\text{Py})$
14	1586	4	1670	0			$\nu_{sk}(\text{Ph})$
15	1584	37	1685	5	1570 s	1572 s	$\nu_{sk}(\text{Py}), \nu_{as}(\text{NO}_2)$
16	1561	14	1650	9	1549 vs	1541 vs	$\nu_{sk}(\text{Py})$
17	1490	6	1551	5	1499 m	1497 m	$\nu_{sk}(\text{Ph})$
18	1466	0	1528	20			$\delta(\text{CH}_2)$
19	1451	22	1514	22	1466 m	1468 m	$\delta(\text{CH}_2), \nu_{sk}(\text{Py})$
20	1444	16	1502	3	1454 m	1450 s	$\nu_{sk}(\text{Ph}), \nu_{sk}(\text{Py})$
21	1426	38	1497	23	1433 s	1431 s	$\nu_{sk}(\text{Py})$
22			1493	22			$\nu_s(\text{NO}_2), \delta(\text{CH}_2)$
23	1379	54			1377 s	1381 s	$\nu_s(\text{NO}_2), \omega(\text{CH}_2)$
24	1368	13	1422	15			$\omega(\text{CH}_2), \beta(\text{Ph-H}), \beta(\text{Py-H})$
25	1320	3	1361	13			$\beta(\text{Ph-H})$
26	1296	47	1331	4	1312 m	1306 s	$\nu_{sk}(\text{Py}), \nu_{sk}(\text{Ph})$
27	1289	5	1332	5			$\nu_{sk}(\text{Ph}), \nu_{sk}(\text{Py})$
28	1281	76	1357	52	1288 s	1294 vs	$\beta(\text{Py-H}), \nu(\text{Py-O})$
29	1230	1	1287	1			$\tau(\text{CH}_2)$
30	1220	29	1266	9	1217 m	1219 m	$\beta(\text{Py-H}), \tau(\text{CH}_2)$
31	1193	0	1247	0			$\beta(\text{Ph-H}), \gamma(\text{CH}_2)$
32	1171	1	1212	1			$\beta(\text{Ph-H})$
33	1150	0	1179	0			$\beta(\text{Ph-H})$
34	1131	2	1177	1			$\beta(\text{Py-H})$
35	1104	22	1160	16	1117 s	1119 s	$\beta(\text{Py-H})$
36	1080	2	1126	1			$\beta(\text{Ph-H})$
37	1056	1	1102	0			$\beta(\text{Py-H})$
38	1024	1	1067	3			$\beta(\text{Ph-H})$
39	1012	18	1089	6		1022 m	$\nu(\text{PhCH}_2\text{-O}), \gamma(\text{Ph-H})$
40	1003	10	1049	0			$\gamma(\text{Ph-H}), \nu(\text{PhCH}_2\text{-O})$
41	989	1	1020	0			$\beta(\text{Ph})$
42	983	0	1029	0			$\gamma(\text{Ph-H})$
43	962	0	1013	0			$\gamma(\text{Py-H})$
44	959	0	1012	0			$\gamma(\text{Ph-H})$
45	903	1	949	0			$\gamma(\text{Ph-H}), \gamma(\text{Py-H})$
46	898	1	941	1	910 w	899 w	$\gamma(\text{Py-H}), \gamma(\text{Ph-H})$
47	857	14	902	11	862 m	866 s	$\delta(\text{NO}_2), \beta(\text{Py})$
48	839	1	880	0			$\gamma(\text{Ph-H})$
49	836	2	876	1		841 w	$\gamma(\text{Ph-H})$
50	803	1	840	0			$\nu(\text{Ph-CH}_2), \beta(\text{Py}), \beta(\text{Ph})$
51	791	18	835	8		795 m	$\gamma(\text{Py-H})$
52	784	1	826	5			$\gamma(\text{Py-H}), \omega(\text{NO}_2)$
53	731	17	758	14		733 s	$\gamma(\text{Ph-H})$
54	715	4	746	2			$\gamma(\text{Py-H})$
55	695	11	717	7	696 s	689 s	$\gamma(\text{Ph-H})$
56	684	8	713	4			$\beta(\text{Py}), \gamma(\text{Ph-H})$
57	619	1	635	1			$\beta(\text{Ph})$
58	608	4	626	1	613 w	613 m	$\beta(\text{Py}), \beta(\text{Ph})$
59	587	1	610	1	590 w	586 w	$\gamma_{sk}(\text{Py})$
60	543	0	563	0	563 vw	546 vw	$\beta(\text{Ph}), \beta(\text{Py})$
61	523	0	550	0			$\gamma_{sk}(\text{Py})$
62	480	2	494	1			$\gamma_{sk}(\text{Py}), \gamma_{sk}(\text{Ph})$
63	448	1	463	1	457 w	463 w	$\gamma_{sk}(\text{Ph}), \gamma_{sk}(\text{Py})$
64	403	0	414	0			$\gamma_{sk}(\text{Ph})$
65	392	1	411	1	417 vw	415 w	$\gamma_{sk}(\text{Py})$

^a Relative absorption intensities normalized with highest peak absorption equal to 100.^b Intensity: vw, very weak; w, weak; m, medium; s, strong; vs very strong.^c Vibrational modes: ν , stretching; δ , scissoring; ω , wagging; ρ , rocking; τ , twisting; γ , out-plane bending; β , in-plane bending; s, symmetric; as, asymmetric; sk, skeletal.

structures with selected structural parameters of the two transition states named **TS1** and **TS2** are also drawn into Fig. 4.

One may have the question that why the nitro group rotates around the N2–C12 bond to adopt a tilted conformation. To

answer the question, we need to examine the structures shown in Fig. 4. Check the structures of **TS1** ($\Phi(\text{NO}_2) = 0^\circ$) that has the nitro group parallel to the pyridine ring, we find that the calculated bond length of N2–C12 bond (1.503 Å from X3LYP calculations) is

longer than the bond length of N2–C12 bond in other structures. In order to explain the bond length difference in these structures, we also did a charge analysis for **BNP**. The NBO charge analysis in Fig. 5 shows that O atom of the 3-benzyloxy moiety and O atom in nitro group all carry much negative formal charges. The approaching two O atoms exists electron–electron repulsions of their lone pairs. As a result, the nitro group in **BNP** adopts a tilted conformation to avoid the repulsion. When $\Phi(\text{NO}_2)$ was restricted to 0° , the calculated distances between O1 and O2 atoms are only 2.59 and 2.56 Å from the X3LYP and M06-2X methods, respectively. However, in the tilted conformation of the X-ray result, O1–O2 distance is enlarged to 2.884(5) Å to minimize the repulsion.

3.3. Vibrational frequency analysis

The vibrational frequencies of **BNP** were calculated and compared with the experimental IR spectra as well as the FT-Raman spectrum. Figs. 6 and 7 show the IR spectra and the FT-Raman spectrum, respectively. Table 3 presents the detailed description of the IR absorption spectra.

3.3.1. Frequencies above 2800 cm^{-1}

The experimental spectrum shows very weak band at 3092 cm^{-1} (in CCl_4 solvent) in FT-IR and a strong band at 3091 cm^{-1} in FT-Raman spectrum, which correspond to the stretching $\nu(\text{Py-H})$ vibrations [24,25]. The prediction of the stretching $\nu(\text{Py-H})$ vibration in 3103 cm^{-1} from the X3LYP method and 3222 cm^{-1} from M06-2X method agree well with the experimental band in FT-IR. The weak bands at 3069 cm^{-1} and 3036 cm^{-1} (in CCl_4 solvent) in FT-IR are assignable to the stretching $\nu(\text{Ph-H})$ vibrations of phenyl groups [26]. The experimental observed bands at 2918 cm^{-1} and 2874 cm^{-1} (in solid state) in FT-IR and 2919 cm^{-1} and 2875 cm^{-1} in FT-Raman are assigned to the asymmetric stretching $\nu_{\text{as}}(\text{CH}_2)$ and symmetric stretching $\nu_{\text{s}}(\text{CH}_2)$ vibrations [26], respectively.

3.3.2. Frequencies from 2800 to 1370 cm^{-1}

In the experimental FT-IR spectrum, the asymmetric stretching $\nu_{\text{as}}(\text{N=O})$ vibrations with medium to strong intensity are located at 1599 cm^{-1} and 1570 cm^{-1} in CCl_4 solvent and at 1599 cm^{-1} and 1572 cm^{-1} in solid state, respectively [25]. The X3LYP functional predicts asymmetric stretching $\nu_{\text{as}}(\text{N=O})$ vibrations are located in 1606 cm^{-1} and 1584 cm^{-1} . From the calculated eigenvectors, it is clearly seen that these bands are connected with $\nu_{\text{as}}(\text{N=O})$ vibrations coupled with pyridine ring vibrations $\nu_{\text{sk}}(\text{Py})$. Two bands for the asymmetric stretching $\nu_{\text{as}}(\text{N=O})$ vibrations are also observed in recently studies on the spectrum of aromatic nitro compounds [25,27]. The deviations between experimental value and X3LYP functional predict value of $\nu_{\text{as}}(\text{N=O})$ are within 15 cm^{-1} , while M06-2X functional overestimates the asymmetric stretching $\nu_{\text{as}}(\text{N=O})$ vibrations. The 1608 cm^{-1} in FT-Raman spectrum is assigned to $\nu_{\text{sk}}(\text{Ph})$ and the asymmetric stretching $\nu_{\text{as}}(\text{N=O})$ vibrations are overlapped in this area. The experimental observed the symmetric stretching $\nu(\text{N=O})$ vibration coupled with wagging $\omega(\text{CH}_2)$ vibrations is 1377 cm^{-1} in CCl_4 solvent and 1381 cm^{-1} in solid state [25]. The X3LYP functional predicted value for this vibration is 1379 cm^{-1} , which agrees well with the experimental data.

3.3.3. Frequencies below 1370 cm^{-1}

The experimental frequency at 1288 cm^{-1} (CCl_4 solvent), with strong intensity, in FT-IR and 1295 cm^{-1} in FT-Raman is connected with the stretching $\nu(\text{Py-O})$ vibration coupled with the in-plane bending $\beta(\text{Py-H})$ [24]. The calculated corresponding frequencies are positioned at 1281 cm^{-1} from the X3LYP method and 1357 cm^{-1} from the M06-2X method, respectively. In the experi-

mental spectrum, the band at 1022 cm^{-1} (in solid state) in FT-IR and 1022 cm^{-1} in FT-Raman is assigned to the stretching $\nu(\text{O-CH}_2\text{Ph})$ mode coupled with out-plane bending $\gamma(\text{Ph-H})$ mode. The corresponding theoretical bands are located at 1012 cm^{-1} from the X3LYP method and 1089 cm^{-1} from the M06-2X method.

The experimental band at 862 cm^{-1} (CCl_4 solvent) in FT-IR and 867 cm^{-1} in FT-Raman spectrum are assigned to $\delta(\text{NO}_2)$ model [25]. The wavenumbers of $\delta(\text{NO}_2)$ model calculated by the X3LYP method (857 cm^{-1}) are in very good agreement with the corresponding experimental data.

The experimental frequencies at 841 cm^{-1} and 795 cm^{-1} in solid state with weak to medium intensity are assigned to the out-plane bending of Ph-H and Py-H. But in CCl_4 solvent, these frequencies are overlapped by $\nu(\text{C-Cl})$ vibration of the solvent. The experimental frequencies at 733 cm^{-1} and 689 cm^{-1} in solid state with strong intensity assigned to the out-plane bending of Ph-H for mono-substituted benzene contain compounds [26].

3.3.4. The prediction of Raman spectra by density functional theory

Fig. 7 show the experimental FT-Raman spectrum compared with theoretical methods predicted Raman spectrum. In the FT-Raman spectrum, the experimental determined frequencies of 3091 cm^{-1} , 3079 cm^{-1} , 3068 cm^{-1} , and 3054 cm^{-1} are assigned to stretching $\nu(\text{Py-H})$ and $\nu(\text{Ph-H})$ vibrations. The X3LYP functional predicted values are 3103 cm^{-1} , 3088 cm^{-1} , 3077 cm^{-1} , and 3062 cm^{-1} , respectively. The deviations between experimental values and X3LYP functional predict values for the specific vibrations are smaller than 20 cm^{-1} . The experimental observed symmetric stretching $\nu(\text{N=O})$ vibration in FT-Raman is 1380 cm^{-1} . The X3LYP functional predicts a very similar values of 1379 cm^{-1} for $\nu(\text{N=O})$. The experimental observed band 1066 cm^{-1} is assigned to the in-plane bending $\beta(\text{Py-H})$, the X3LYP functional predict value for this vibration is 1056 cm^{-1} and M06-2X functional predict value is 1102 cm^{-1} . From the analysis, we can see that the band positions and intensities of the Raman-active vibrations predicated by X3LYP functional are well-reproduced the experimental results.

4. Conclusions

In conclusion, the molecular structure of **BNP** was investigated both experimentally and theoretically. A disordered nitro group with a large dihedral angle of $66.4(4)^\circ$ between it and its connected pyridyl group as well as a centrosymmetric π -stacking molecular pair has been found in the crystalline state. The following theoretical analysis reveals that the tilt of the nitro group can enlarge the distance between the O atoms of the 3-benzyloxy and the nitro groups from 2.59 to 2.88 Å and thus diminishes the repulsion between them. An energetically favored dihedral angle of $\Phi(\text{NO}_2) = 53.9^\circ$ from the X3LYP method coincides well with the experimental data of $\Phi(\text{NO}_2) = 66.4(4)^\circ$. The existing two conformational isomers of 3-benzyloxy-2-nitropyridine with equal energy explain well the disorder of the nitro group at room temperature. The calculated rotational barrier height of the nitro group is only 1.6 kcal mol^{-1} . In addition, the vibrational frequency analyses indicate that the X3LYP method can predict the vibrational bands more closely than the M06-2X method.

Acknowledgements

This work was supported by Grants from the NSFC (Nos. 20834002 and 20872109) and the Innovation Foundation of Tianjin University. Parts of this work are also supported by High Performance Computing Center of Tianjin University, China. The authors

would like to express their thanks to Prof. Mingyi Tang of Tianjin University of Commerce for his helpful discussion.

Appendix A. Supplementary material

Supplementary data associated with this article can be found, in the online version, at <http://dx.doi.org/10.1016/j.molstruc.2012.05.064>.

References

- [1] T.V. Rybalova, V.F. Sedova, Y.V. Gatilov, O.P. Shkurko, *Chem. Heterocycl. Compd.* 34 (1998) 1161–1165.
- [2] J. Trotter, *Acta Crystallogr.* 12 (1959) 884–888.
- [3] R. Moreno-Fuquen, J. Valderrama-Naranjo, A.M. Montano, *Acta Crystallogr. C* 55 (1999) 218–220.
- [4] C.M.L. Vande Velde, H.J. Geise, F. Blockhuys, *Acta Crystallogr. E* 60 (2004) o199–o200.
- [5] J. Trotter, *Acta Crystallogr.* 13 (1960) 95–99.
- [6] J. Trotter, *Acta Crystallogr.* 12 (1959) 605–607.
- [7] D.J.A. De Ridder, H. Schenk, D. Döpp, *Acta Crystallogr. C* 49 (1993) 1970–1971.
- [8] M. Yamakawa, T. Kubota, K. Ezumi, Y. Mizuno, *Spectrochim. Acta A* 30 (1974) 2103–2119.
- [9] G.-Y. Yeap, H.-K. Fun, S.-B. Teo, S.-G. Teoh, *Acta Crystallogr. C* 48 (1992) 1898–1900.
- [10] D.E. Lynch, I. McClenaghan, *Acta Crystallogr. E* 57 (2001) o83–o84.
- [11] S.Z. Hu, D.S. Shi, S.X. Li, Y.C. Yang, *Acta Crystallogr. C* 48 (1992) 1597–1599.
- [12] T. Nakamura, K. Takeuchi, JP Patent 2003-238832A, 2003.
- [13] X. Xu, W.A. Goddard III, *Proc. Natl. Acad. Sci. USA* 101 (2004) 2673–2677.
- [14] X. Xu, Q. Zhang, R.P. Muller, W.A. Goddard III, *J. Chem. Phys.* 122 (2005) 014105.
- [15] Y. Zhao, D. Truhlar, *Theor. Chem. Acc.* 120 (2008) 215–241.
- [16] G.M. Sheldrick, SHELXS-97 and SHELXL-97, Program for X-ray Crystal Structure Determination, University of Göttingen, Germany, 1997.
- [17] M.J. Frisch, G.W. Trucks, H.B. Schlegel, G.E. Scuseria, M.A. Robb, J.R. Cheeseman, G. Scalmani, V. Barone, B. Mennucci, G.A. Petersson, H. Nakatsuji, M. Caricato, X. Li, H.P. Hratchian, A.F. Izmaylov, J. Bloino, G. Zheng, J.L. Sonnenberg, M. Hada, M. Ehara, K. Toyota, R. Fukuda, J. Hasegawa, M. Ishida, T. Nakajima, Y. Honda, O. Kitao, H. Nakai, T. Vreven, J.A. Montgomery, Jr., J.E. Peralta, F. Ogliaro, M. Bearpark, J.J. Heyd, E. Brothers, K.N. Kudin, V.N. Staroverov, T. Keith, R. Kobayashi, J. Normand, K. Raghavachari, A. Rendell, J.C. Burant, S.S. Iyengar, J. Tomasi, M. Cossi, N. Rega, J.M. Millam, M. Klene, J.E. Knox, J.B. Cross, V. Bakken, C. Adamo, J. Jaramillo, R. Gomperts, R.E. Stratmann, O. Yazyev, A.J. Austin, R. Cammi, C. Pomelli, J.W. Ochterski, R.L. Martin, K. Morokuma, V.G. Zakrzewski, G.A. Voth, P. Salvador, J.J. Dannenberg, S. Dapprich, A.D. Daniels, O. Farkas, J. B. Foresman, J.V. Ortiz, J. Cioslowski, D.J. Fox, *Gaussian 09, Revision A.02*, Gaussian, Inc., Wallingford, CT, 2009.
- [18] R. Krishnan, J.S. Binkley, R. Seeger, J.A. Pople, *J. Chem. Phys.* 72 (1980) 650–654.
- [19] A.E. Reed, R.B. Weinstock, F. Weinhold, *J. Chem. Phys.* 83 (1985) 735–746.
- [20] E.D. Glendening, J.K. Badenhoop, A.E. Reed, J.E. Carpenter, J.A. Bohmann, C.M. Morales, Weinhold, F. NBO 5.9, Theoretical Chemistry Institute, University of Wisconsin, Madison, WI, 2011.
- [21] F. Teixeira, A. Melo, M.N.D.S. Cordeiro, *J. Chem. Phys.* 133 (2010) 114109.
- [22] M. Melguizo, A. Quesada, J.N. Low, C. Glidewell, *Acta Crystallogr. B* 59 (2003) 263–276.
- [23] C. Glidewell, J.N. Low, A. Marchal, A. Quesada, *Acta Crystallogr. C* 59 (2003) o454–o460.
- [24] F. Uzun, V. Güçlü, A. Sağlam, *Spectrochim. Acta A* 70 (2008) 524–531.
- [25] N. Sundaraganesan, S. Ilakiamani, H. Saleem, P.M. Wojciechowski, D. Michalska, *Spectrochim. Acta A* 61 (2005) 2995–3001.
- [26] B. Stuart, *Infrared Spectroscopy: Fundamentals and Applications*, J. Wiley, Chichester, England, Hoboken, NJ, 2004.
- [27] V. Arjunan, P. Ravindran, K. Balakrishnan, R. Santhanam, S. Mohan, *J. Mol. Struct.* 1016 (2012) 82–96.